ARTICLE



¹³C and ¹⁵N chemical shift assignments of A117V and M129V human Y145Stop prion protein amyloid fibrils

Hanh H. Dao¹ · May Z. Hlaing¹ · Yixuan Ma¹ · Krystyna Surewicz² · Witold K. Surewicz² · Christopher P. Jaroniec¹

Received: 27 June 2020 / Accepted: 24 October 2020 / Published online: 29 October 2020 © Springer Nature B.V. 2020

Abstract

The C-terminally truncated Y145Stop variant of prion protein (PrP23-144) has been linked to a heritable prionopathy in humans and is also capable of triggering a transmissible prion disease in mice. PrP23-144 can be converted from soluble monomeric form to amyloid under physiological conditions, providing an in vitro model for investigating the molecular basis of amyloid strains and cross-seeding barriers. Here, we use magic-angle spinning solid-state NMR to establish the sequential backbone and sidechain ¹³C and ¹⁵N chemical shift assignments for amyloid fibrils formed by the A117V and M129V mutants of human PrP23-144, which in the context of full length PrP in vivo are among the specific residues associated with development of Gerstmann–Straüssler–Scheinker disease. The chemical shift data are utilized to identify amino acids comprising the rigid amyloid core regions and to predict the protein secondary structures for human PrP23-144 A117V and M129V fibrils.

Keywords Prion protein · Amyloid · Gerstmann-Straüssler-Scheinker disease · Magic-angle spinning · Solid-state NMR

Biological context

Transmissible spongiform encephalopathies (TSEs) or prion diseases are a family of fatal neurodegenerative disorders in mammals that include Creutzfeldt–Jakob disease in humans, scrapie in sheep and "mad cow" disease, with their pathogenesis occurring through accumulation in the central nervous system of toxic, β -sheet rich amyloid aggregates of scrapie-like prion protein (PrPSc) formed by misfolding of the predominantly α -helical monomeric cellular protein (PrPC) (Prusiner 1998). Human prion diseases typically present sporadically but can also be inherited—the latter

May Z. Hlaing and Yixuan Ma have contributed equally to this work.

Accession numbers Chemical shift assignments for A117V and M129V huPrP23-144 amyloid fibrils have been deposited in the BioMagResBank (https://www.bmrb.wisc.edu) under accession numbers 50,312 and 50,313, respectively.

- Christopher P. Jaroniec jaroniec.1@osu.edu
- Department of Chemistry and Biochemistry, The Ohio State University, Columbus, OH 43210, USA
- Department of Physiology and Biophysics, Case Western Reserve University, Cleveland, OH 44106, USA

include diseases such as fatal familial insomnia and Gerstmann–Straüssler–Scheinker (GSS) disease (Pirisinu et al. 2016; Prusiner 1998). GSS disease is caused by various pathogenic PrP mutations including P102L, P105L, A117V, and F198S, which are most often found in combination with Met/Val polymorphism at codon 129 (Tagliavini et al. 2001; Young et al. 1997). Furthermore, most GSS disease subtypes are associated with amyloid fibrils consisting of significantly shorter 6–8 kDa peptides typically spanning PrP residues ~70–150 (Cracco et al. 2019; Piccardo et al. 2001; Tagliavini et al. 2001).

The Y145Stop PrP variant (PrP23-144), which is associated with the development of familial PrP cerebral amyloid angiopathy in humans (Ghetti et al. 1996; Kitamoto et al. 1993) and has been demonstrated to trigger a transmissible prion disease in mice (Choi et al. 2016), is an established in vitro model for studying amyloid transmissibility barriers (Kundu et al. 2003; Surewicz et al. 2006). PrP23-144 also provides a valuable model for investigating the structural and kinetic effects of many GSS-associated mutations, given that this PrP fragment contains most of the residues comprising the protease-resistant core in amyloid deposits found in GSS disease patients (Kundu et al. 2003; Surewicz et al. 2006).

Here we extend our previous structural and dynamic magic angle spinning solid-state NMR studies of mammalian PrP23-144 variants (Aucoin et al. 2019; Helmus



et al. 2008, 2010, 2011; Jones et al. 2011; Shannon et al. 2019; Theint et al. 2017a, b, 2018) to determine the nearly complete sequential backbone and sidechain ¹³C and ¹⁵N chemical shift assignments and residue-specific molecular conformations for amyloids formed by the A117V and M129V human (hu) PrP23-144 variants. In all GSS A117V disease cases to date, valine at position 117 has been found in conjunction with valine at position 129 in either the 129VV or 129MV genotype (Cracco et al. 2019; Piccardo et al. 2001; Tagliavini et al. 2001). In an earlier study of the role of N-terminal familial mutations in huPrP23-144 amyloid propagation, Surewicz and co-workers (Jones et al. 2006) found that the lag phase for conversion to amyloid was somewhat (~10-20%) shorter for V129 relative to M129 huPrP23-144 while the A117V mutation alone had a negligible effect on the kinetics of huPrP23-144 conversion. Additionally, low resolution FTIR studies revealed that M129 and V129 huPrP23-144 amyloids had secondary structures similar to the corresponding A117V mutants and that M129 and V129 huPrP23-144 fibrils exhibited distinct conformational features which were not transmissible by cross-seeding (Jones et al. 2006). The present study enables the impact of residues 117 and 129 on huPrP23-144 confirmation to be evaluated with site-specific detail and establishes a foundation for continued high-resolution structural analysis of these PrP23-144 variants.

Methods and experiments

Protein expression and purification

The plasmid encoding A117V huPrP23-144, containing an N-terminal His₆-tag and thrombin cleavage site, was described previously (Theint et al. 2017b). A similar construct for the expression of M129V huPrP23-144 was generated by site-directed mutagenesis using the wild-type (wt) huPrP23-144 plasmid (Vanik et al. 2004), Herculase II Fusion DNA Polymerase (Agilent), and the following primers: 5'-CCTTGGCGGCTACGTGCTGGGAAGTGC-3' and 5'-GCACTTCCCAGCACGTAGCCGCCAAGG-3', and confirmed by Sanger sequencing (Genewiz).

Proteins were expressed and purified using previously published protocols (Theint et al. 2017b). *E. coli* BL21 (DE3) competent cells were transformed with the plasmid encoding for the mutation of interest. The transformed cells were grown at 37 °C, 250 rpm in Luria–Bertani medium with 0.1 mg/mL ampicillin to OD_{600} of ~ 1.0. Cells were collected via centrifugation at 3,500 rpm, 4 °C for 15 min then resuspended in the same volume of M9 minimal medium with 0.1 mg/mL ampicillin, containing 1 g/L 15 N ammonium chloride and 3 g/L of 13 C glucose as the sole nitrogen and carbon sources, respectively.

Protein expression was induced by adding isopropyl β-D-thiogalactoside to a final concentration of 1 mM, and cells were allowed to resume growth at 37 °C, 250 rpm for 16 h. Cells were then collected as a pellet via centrifugation at 4900 rpm, 4 °C for 20 min, and resuspended in ~ 100 mL of lysis buffer (6 M GdmCl, 10 mM Tris-HCl, 100 mM potassium phosphate, pH 8.0). Cells were lysed via sonication followed by 30 min of centrifugation at 20,000 rpm, 4 °C to remove cell debris, and the protein in the supernatant was purified using nickel-nitrilotriacetic acid (Ni-NTA) superflow resin (Qiagen) and nickel-ion affinity chromatography. The N-terminal His6-tag was cleaved using biotinylated thrombin (Novagen), followed by thrombin removal using streptavidin-agarose beads and by dialysis against ultrapure Milli-Q water to remove free His6-tag. Protein purity was confirmed by SDS/PAGE and MALDI-MS, and proteins were lyophilized and stored at -20 °C.

Preparation of amyloid fibrils

Lyophilized A117V and M129V huPrP23-144 proteins were dissolved in ultrapure Milli-Q water at a concentration of 5 mg/mL (~400 μM). 1.0 M potassium phosphate pH 6.4 buffer was then added to a final concentration of 50 mM, and the protein solutions were incubated under quiescent conditions at 25 °C for 48 h with only gentle inversion of the sample tubes every 12 h to ensure thorough mixing (Theint et al. 2017a, b). The resulting suspensions were centrifuged to collect the fibrils, and the fibrils (~10–15 mg per sample) were washed with several aliquots of 50 mM potassium phosphate pH 6.4 buffer containing 0.02% (v/v) sodium azide and transferred via centrifugation to 3.2 mm Bruker zirconia rotors. The samples were stored in a refrigerator at 4 °C when not in use.

Atomic force microscopy

Fibrils used for the solid-state NMR measurements were routinely characterized by atomic force microscopy (AFM). Small aliquots of the fibril suspensions above were diluted 1:5 with ultrapure Milli-Q water and deposited onto freshly cleaved mica substrates (Ted Pella, Inc.), incubated for 2 min, rinsed with two 50 μ L aliquots of Milli-Q water to remove salts and unbound fibrils, and air-dried. Imaging was performed in tapping mode in air using a Bruker Dimension Icon AFM and high-sensitivity silicone Bruker RTESPA MPP-11120-10 probes with a nominal spring constant of 40 N/m and nominal tip radius of 8 nm. The images were processed with the Bruker NanoScope Analysis software using interactive plane fitting.



Solid-state NMR spectroscopy

NMR spectra were recorded on an 800 MHz Bruker spectrometer, equipped with a 3.2 mm E^{free} triple resonance (¹H-¹³C-¹⁵N) magic angle spinning (MAS) probe. The spinning frequency and temperature were actively controlled at 11.111 kHz and 5 °C, respectively. The sequential ¹³C and ¹⁵N resonance assignments were determined using a set of standard 2D and 3D chemical shift correlation experiments including: 2D ¹⁵N-¹³Cα (NCA), $2D^{-15}N^{-13}C'$ (NCO). $2D^{-15}N^{-13}C\alpha^{-13}CX$ (N(CA)CX). $2D^{-15}N^{-13}C'^{-13}CX$ (N(CO)CX), $3D^{-15}N^{-13}C\alpha^{-13}CX$ (NCACX), 3D 15N-13C'-13CX (NCOCX) and 3D 13 C α - 15 N- 13 C'- 13 CX (CAN(CO)CX). NMR spectra were processed with Bruker TopSpin 3.7 software and NMR-Pipe (Delaglio et al. 1995) and analyzed using Sparky (Goddard and Kneller 2006), and data were collected for several independent fibril preparations to confirm sample reproducibility.

Assignments and data deposition

AFM images of A117V and M129V huPrP24-144 fibrils (Fig. 1b) show that both mutants readily assemble into micron-length amyloid fibrils with morphologies similar to wt huPrP23-144 fibrils, in agreement with earlier studies (Jones et al. 2006; Theint et al. 2017a). Interestingly, the ¹⁵N-¹³Cα fingerprint spectra of A117V and M129V fibrils (Fig. 1c) display significant ¹³C and ¹⁵N chemical shift differences relative to each other and to wt huPrP23-144 fibrils: the differences in backbone ¹³C and ¹⁵N chemical shifts between the different fibril samples are quantified in Fig. 2a. Additionally, the A117V and M129V fibrils both exhibit significantly less variation in resonance intensities in comparison to the wt fibrils (Fig. 2b). Collectively, these spectral differences suggest that mutations at positions 117 and 129 have a significant impact on the conformation and flexibility of the huPrP23-144 amyloid core region with the two mutants adopting distinct three-dimensional structures

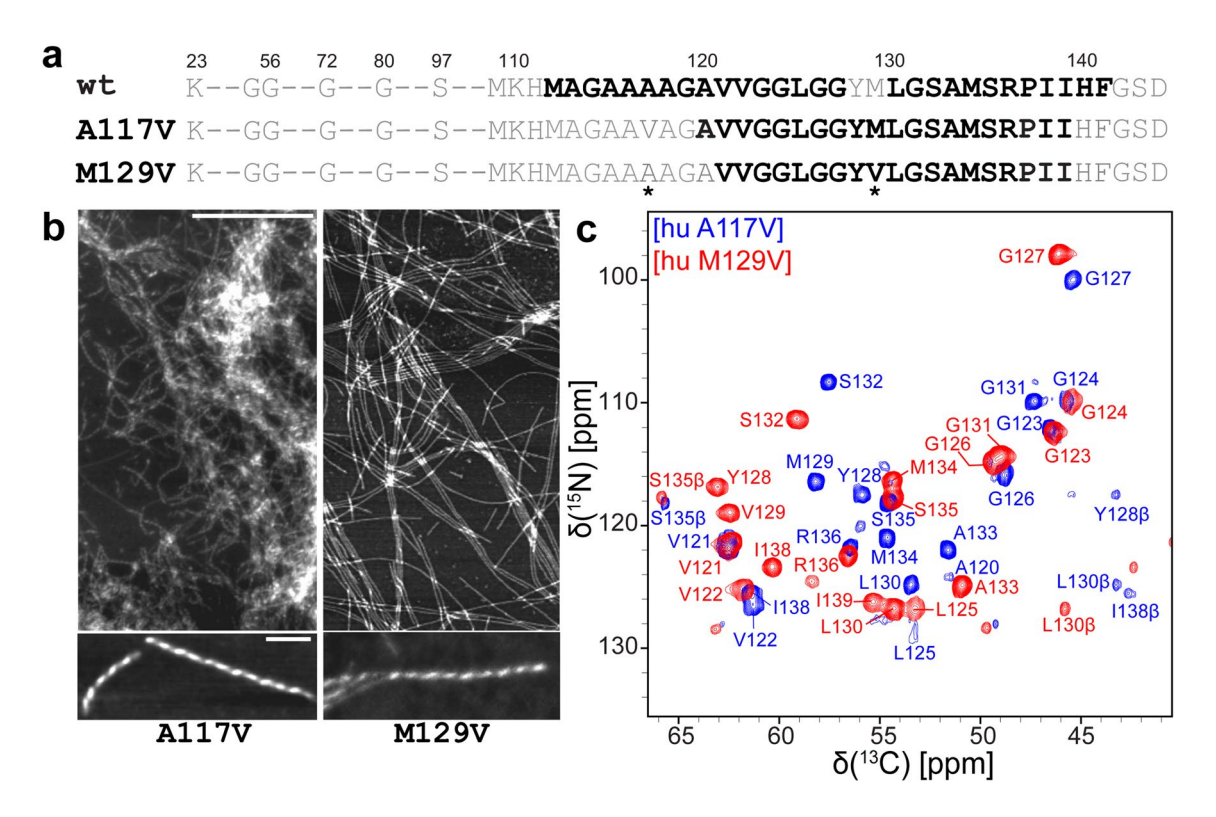


Fig. 1 a Amino acid sequences of huPrP23-144 (wt), and huPrP23-144 A117V (A117V) and huPrP23-144 M129V (M129V) variants with the mutated residues indicated by asterisks. Largely immobile amyloid core residues detectable in conventional solid-state NMR spectra are shown in bold black font and conformationally flexible residues are shown in grey front. **b** Representative atomic force microscopy images of A117V and M129V amyloid fibrils used for the solid-state NMR measurements. The top panels show wide-field images containing fibril bundles, with close up views of representative single fibrils shown in the bottom panels. The scale bars in the upper and lower panels correspond to 1 µm and 100 nm, respec-

tively. **c** Assigned two-dimensional 800 MHz $^{15}N^{-13}C\alpha$ solid-state NMR spectra of A117V (blue contours) and M129V (red contours) huPrP23-144 amyloid fibrils recorded at 11.111 kHz MAS frequency. Note that $^{15}N^{-13}C\beta$ correlations for several residues are also observed as indicated, although with significantly lower intensity relative to corresponding $^{15}N^{-13}C\alpha$ cross-peaks, due to partial through-space magnetization transfer from ^{15}N to $^{13}C\beta$ during the band-selective cross-polarization period. Each spectrum was recorded with acquisition times of 12 ms (t_1 , ^{15}N) and 30 ms (t_2 , ^{13}C) and a total measurement time of about 24 h. Cross-peaks are drawn with the lowest contour at about 15 times the root mean square noise level



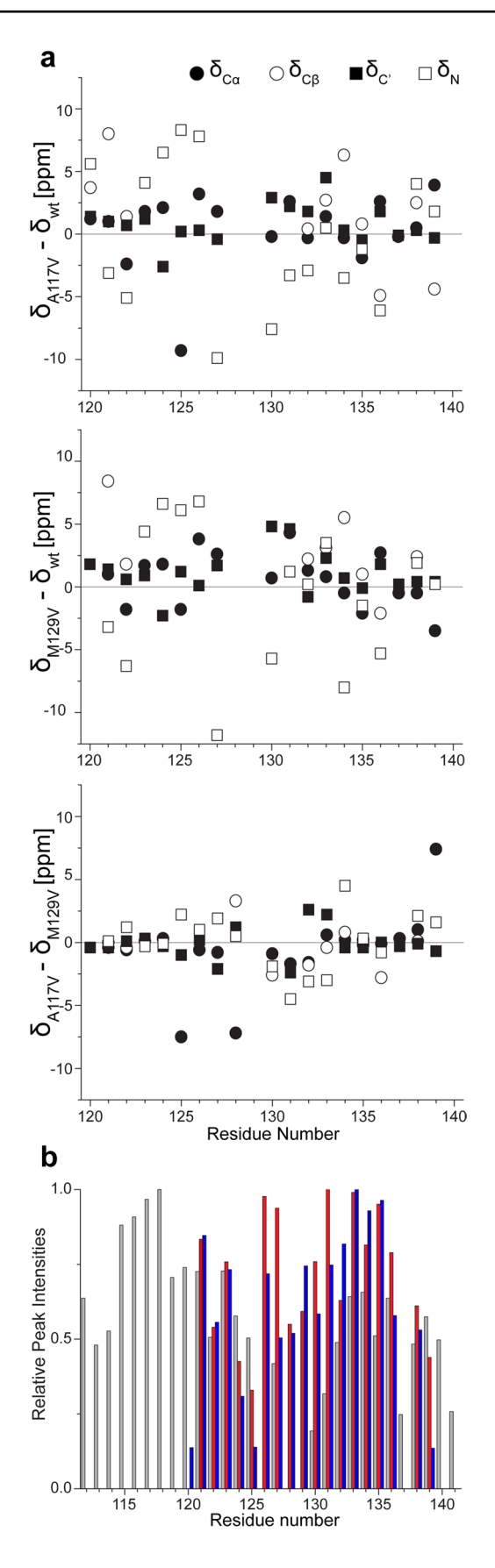
48 H. H. Dao et al.

Fig. 2 a Residue-specific chemical shift differences between A117V, ▶ M129V and wt huPrP23-144 fibrils, plotted for residues observed in both the wt and mutant fibrils (and excluding the mutated residues). The chemical shifts differences are shown as solid circles, open circles, solid squares and open squares for $C\alpha$, $C\beta$, C', and N, respectively. The average absolute chemical shift differences between wt and A117V, between wt and M129V, and between the two mutants are respectively: 2.04 ± 2.05 ppm, 1.85 ± 1.16 ppm, and 1.83 ± 2.56 ppm for $C\alpha$; 3.51 ± 2.32 ppm, 3.31 ± 2.29 ppm and 1.28 ± 1.16 ppm for $C\beta$; 1.25 ± 1.16 ppm, 1.45 ± 1.34 ppm and 0.89 ± 0.86 ppm for C'; 4.78 ± 2.57 ppm, 4.54 ± 3.06 ppm and 1.71 ± 1.37 ppm for N. **b** Normalized relative intensities for individual resonances in 15 N- 13 C solid-state NMR spectra of wt (grey), A117V (blue) and M129V (in red) huPrP23-144 amyloid fibrils plotted as a function of residue number

(see below for additional discussion). The latter observation is also broadly consistent with distinct FTIR amide I region spectra previously reported for A117V and M129V huPrP23-144 fibrils (Jones et al. 2006).

Given that the fingerprint spectra for A117V and M129V fibrils exhibit minimal overlap among the cross-peaks, the sequential resonance assignments of the rigid core residues for both amyloids could be largely established by using 2D N(CA)CX and N(CO)CX spectra (Fig. 3a, b). Specifically, backbone and side-chain signals were observed for only 19 and 20 residues (out of ~122 total) for hu M129V and hu A117V fibrils, respectively, suggesting that, in analogy to wt huPrP23-144 fibrils, the rigid amyloid core regions for these mutants are quite compact (Helmus et al. 2008). The rigid core regions for A117V and M129V fibrils were found to span residues 120-139 and 121-139, respectively, with ~ 100-residue N-terminal domains and ~ five C-terminal residues not detectable for either amyloid due to increased conformational flexibility (Helmus et al. 2010). Remarkably, both mutations effectively shorten the size of the amyloid core region observed for wt huPrP23-144 fibrils by $\sim 9-10$ residues ($\sim 30-40\%$) and do not appear to contain segments within their cores that exhibit significant conformational flexibility (e.g., such as the G127-L130 stretch in wt huPrP23-144 amyloid). The initial assignments were confirmed and further extended by using a set of 3D ¹⁵N-¹³C-¹³C correlation spectra, resulting in nearly complete (96% for A117V and 95% for M129V) ¹³C and ¹⁵N backbone and side-chain assignments for residues that are detectable in conventional experiments based on dipolar coupling-driven magnetization transfers as discussed above—Fig. 3c shows representative strips from 3D NCACX, NCOCX, and CAN(CO)CX datasets, illustrating sequential backbone connectivity for residues G127-S132 in A117V huPrP23-144 fibrils.

The secondary structures for the A117V and M129V huPrP23-144 fibrils were predicted from the experimental ¹³C and ¹⁵N chemical shifts to evaluate the similarities and differences in backbone conformation between the two





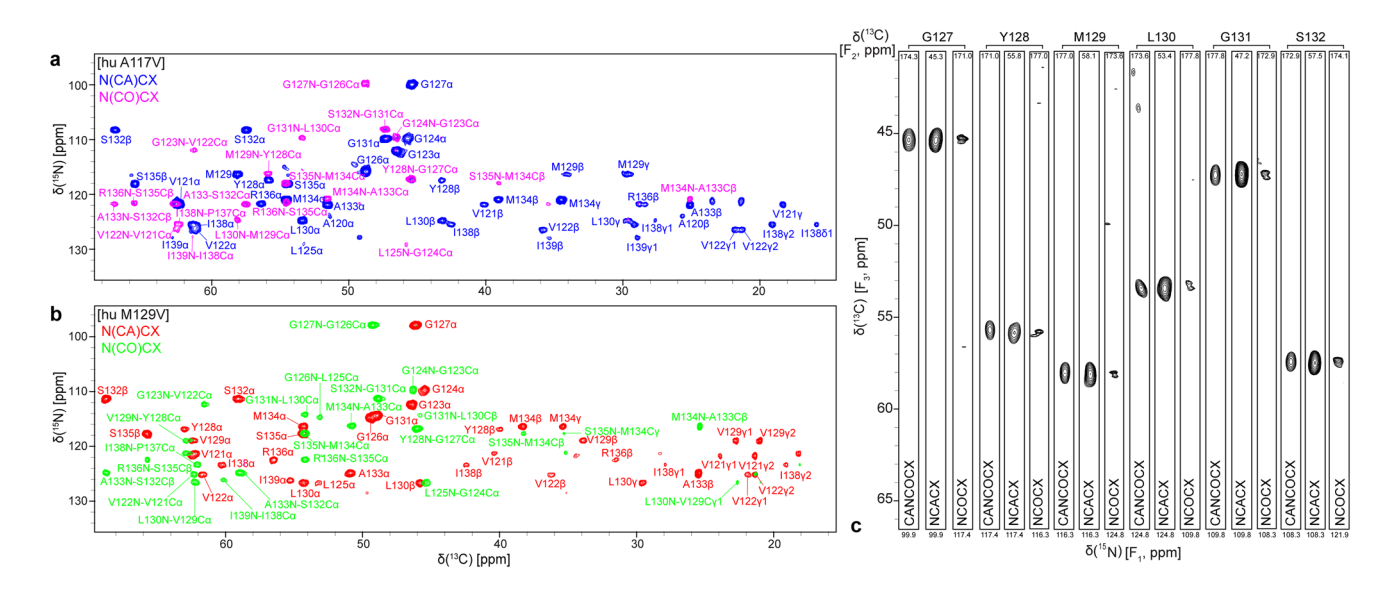


Fig. 3 Assigned two-dimensional 800 MHz 2D N(CA)CX and 2D N(CO)CX solid-state NMR spectra of **a** A117V and **b** M129V huPrP23-144 amyloid fibrils. The side-chain assignments for valines are not stereospecific. **c** Representative strips from 800 MHz 3D

CAN(CO)CX, NCACX, and NCOCX spectra for A117V fibrils showing sequential connectivity for residues G127-S132. Strips are labeled by residue number according to the 15 N frequency (F_1), with the 13 C frequencies (F_2) indicated at the top of each strip

mutants and wt huPrP23-144 amyloid. For both mutants, the TALOS-N program (Shen and Bax 2013) was used to obtain the residue-specific ϕ and ψ backbone dihedral angles and β -sheet probabilities for the amyloid core residues (Fig. 4), with residues having β -sheet probabilities of 50% or more classified as comprising the β -strands. In addition, a few residues with β -sheet probabilities below 50% were also classified as comprising the β -strands provided that: (1) all of their ϕ and ψ predictions fell into the β -strand region of the Ramachandran space and/or (2) they were flanked by residues with β -sheet probabilities of 50% or higher. The secondary structure prediction, summarized in Fig. 4a, suggests that A117V and M129V huPrP23-144 fibrils contain two β -strands separated by a non- β segment—for both amyloids the first β -strand spans residues

121–125 while the second β-strand consists of residues 128–135 for A117V and 130–139 for M129V fibrils. Interestingly, for M129V amyloid the two β-strands coincide largely with the two C-terminal β-strands in wt huPrP23-144 fibrils although, as noted above, the non- β segment containing residues ~ 127–130 in M129V fibrils does not appear to exhibit major conformational flexibility as in wt huPrP23-144 amyloid. Altogether, the results of our studies indicate that the precise identities of residues 117 and 129 significantly influence the conformation and flexibility of huPrP23-144 amyloid and provide a foundation for high-resolution structural analysis of these PrP23-144 variants and, more broadly, the evaluation of potential structural roles played by these residues in the context of PrP misfolding diseases.



50 H. H. Dao et al.

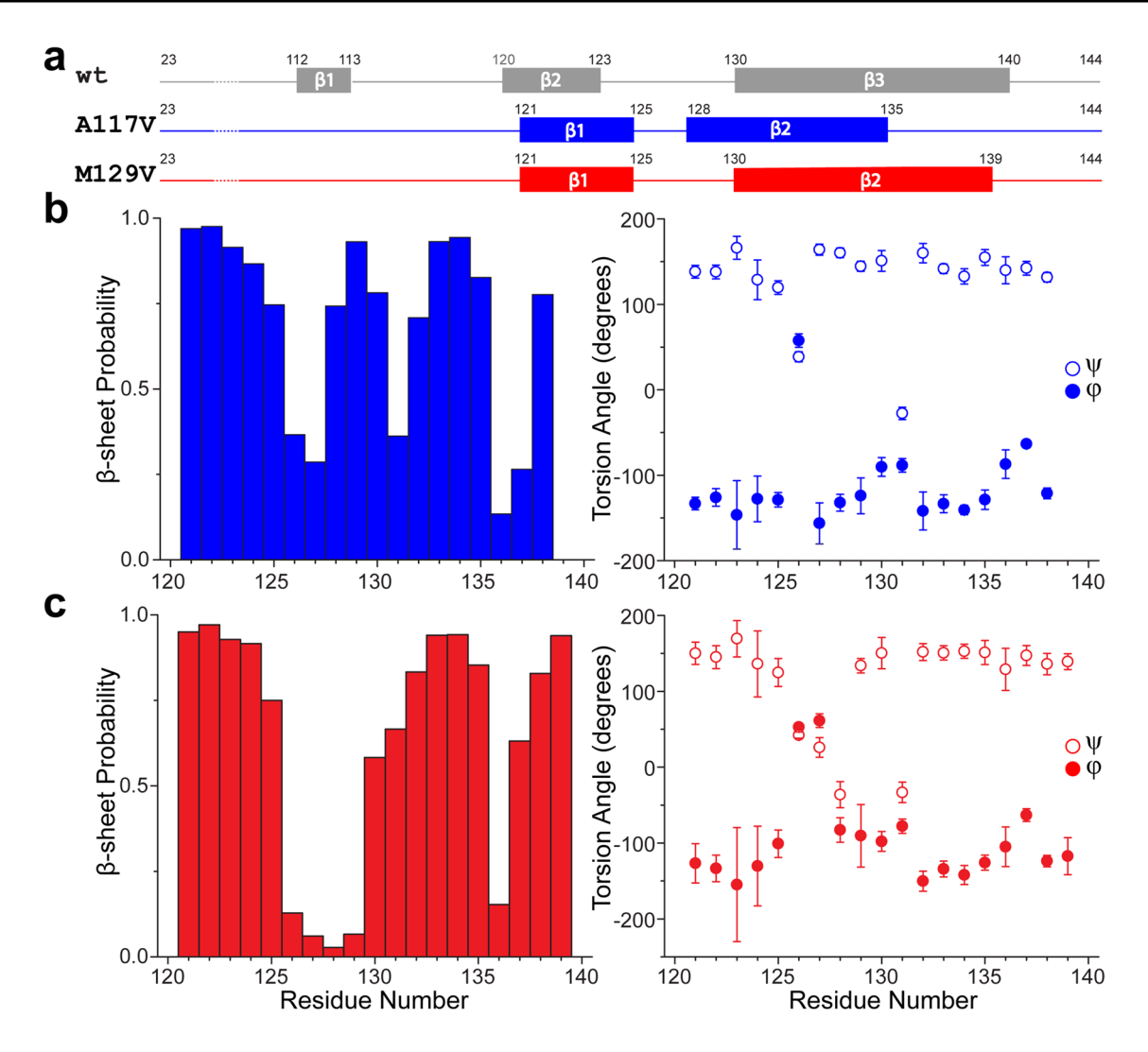


Fig. 4 a Summary of the secondary structure analysis for wt, A117V and M129V huPrP23-144 amyloid fibrils based on the assigned 13 C and 15 N chemical shifts (see text for details). **b** (Left) The β-sheet probability and (right) backbone φ (filled circles) and ψ (open cir-

cles) torsion angle values for b A117V and c M129V huPrP23-144 amyloid fibrils as a function of residue number predicted using the TALOS-N software (Shen and Bax 2013)

Acknowledgements This research was supported by NIH (Grants R01GM094357 and S10OD012303 to C.P.J., P01AI106705 and R01NS083687 to W.K.S., and RF1AG061797 to W.K.S. and C.P.J.), and NSF (Grant MCB-1715174 to C.P.J.).

References

Aucoin D, Xia Y, Theint T, Nadaud PS, Surewicz K, Surewicz WK, Jaroniec CP (2019) Protein-solvent interfaces in human Y145Stop prion protein amyloid fibrils probed by paramagnetic solid-state NMR spectroscopy. J Struct Biol 206(1):36–42. https://doi. org/10.1016/j.jsb.2018.04.002

Choi J-K, Cali I, Surewicz K, Kong Q, Gambetti P, Surewicz WK (2016) Amyloid fibrils from the N-terminal prion protein fragment

are infectious. Proc Natl Acad Sci USA 113(48):13851–13856. https://doi.org/10.1073/pnas.1610716113

Cracco L, Xiao X, Nemani SK, Lavrich J, Cali I, Ghetti B, Notari S, Surewicz WK, Gambetti P (2019) Gerstmann-Sträussler-Scheinker disease revisited: accumulation of covalently-linked multimers of internal prion protein fragments. Acta Neuropathol Commun 7(1):85. https://doi.org/10.1186/s40478-019-0734-2

Delaglio F, Grzesiek S, Vuister GW, Zhu G, Pfeifer J, Bax A (1995) NMRPipe: a multidimensional spectral processing system based on UNIX pipes. J Biomol NMR 6(3):277–293. https://doi. org/10.1007/BF00197809

Ghetti B, Piccardo P, Spillantini MG, Ichimiya Y, Porro M, Perini F, Kitamoto T, Tateishi J, Seiler C, Frangione B, Bugiani O, Giaccone G, Prelli F, Goedert M, Dlouhy SR, Tagliavini F (1996) Vascular variant of prion protein cerebral amyloidosis with taupositive neurofibrillary tangles: the phenotype of the stop codon 145 mutation in PRNP. Proc Natl Acad Sci 93(2):744–748. https://doi.org/10.1073/pnas.93.2.744



- Goddard TD, Kneller DG (2006) SPARKY 3. University of California, San Francisco
- Helmus JJ, Surewicz K, Nadaud PS, Surewicz WK, Jaroniec CP (2008) Molecular conformation and dynamics of the Y145Stop variant of human prion protein in amyloid fibrils. Proc Natl Acad Sci 105(17):6284–6289. https://doi.org/10.1073/pnas.0711716105
- Helmus JJ, Surewicz K, Surewicz WK, Jaroniec CP (2010) Conformational flexibility of the Y145Stop human prion protein amyloid fibrils probed by solid-state nuclear magnetic resonance spectroscopy. J Am Chem Soc 132(7):2393–2403. https://doi.org/10.1021/ja909827v
- Helmus JJ, Surewicz K, Apostol MI, Surewicz WK, Jaroniec CP (2011) Intermolecular alignment in Y145Stop human prion protein amyloid fibrils probed by solid-state NMR spectroscopy. J Am Chem Soc 133(35):13934–13937. https://doi.org/10.1021/ja206469q
- Jones EM, Surewicz K, Surewicz WK (2006) Role of N-terminal familial mutations in prion protein fibrillization and prion amyloid propagation in vitro. J Biol Chem 281(12):8190–8196. https://doi.org/10.1074/jbc.M513417200
- Jones EM, Wu B, Surewicz K, Nadaud PS, Helmus JJ, Chen S, Jaroniec CP, Surewicz WK (2011) Structural polymorphism in amyloids: new insights from studies with Y145Stop prion protein fibrils.
 J Biol Chem 286:42777–42784. https://doi.org/10.1074/jbc. M111.302539
- Kitamoto T, Iizuka R, Tateishi J (1993) An amber mutation of prion protein in Gerstmann-Sträussler syndrome with mutant PrP plaques. Biochem Biophys Res Commun 192(2):525–531. https://doi.org/10.1006/bbrc.1993.1447
- Kundu B, Maiti NR, Jones EM, Surewicz KA, Vanik DL, Surewicz WK (2003) Nucleation-dependent conformational conversion of the Y145Stop variant of human prion protein: structural clues for prion propagation. Proc Natl Acad Sci 100(21):12069–12074. https://doi.org/10.1073/pnas.2033281100
- Piccardo P, Liepnieks JJ, William A, Dlouhy SR, Farlow MR, Young K, Nochlin D, Bird TD, Nixon RR, Ball MJ, DeCarli C, Bugiani O, Tagliavini F, Benson MD, Ghetti B (2001) Prion proteins with different conformations accumulate in Gerstmann-Sträussler-Scheinker disease caused by A117V and F198S mutations. Am J Pathol 158(6):2201–2207. https://doi.org/10.1016/S0002-9440(10)64692-5
- Pirisinu L, Di Bari MA, D'Agostino C, Marcon S, Riccardi G, Poleggi A, Cohen ML, Appleby BS, Gambetti P, Ghetti B, Agrimi U, Nonno R (2016) Gerstmann-Sträussler-Scheinker disease subtypes efficiently transmit in bank voles as genuine prion diseases. Sci Rep 6:20443. https://doi.org/10.1038/srep20443
- Prusiner SB (1998) Prions. Proc Natl Acad Sci 95(23):13363–13383. https://doi.org/10.1073/pnas.95.23.13363

- Shannon MD, Theint T, Mukhopadhyay D, Surewicz K, Surewicz WK, Marion D, Schanda P, Jaroniec CP (2019) Conformational dynamics in the core of human Y145Stop prion protein amyloid probed by relaxation dispersion NMR. ChemPhysChem 20(2):311–317. https://doi.org/10.1002/cphc.201800779
- Shen Y, Bax A (2013) Protein backbone and sidechain torsion angles predicted from NMR chemical shifts using artificial neural networks. J Biomol NMR 56(3):227–241. https://doi.org/10.1007/ s10858-013-9741-v
- Surewicz WK, Jones EM, Apetri AC (2006) The emerging principles of mammalian prion propagation and transmissibility barriers: insight from studies in vitro. Acc Chem Res 39(9):654–662. https://doi.org/10.1021/ar050226c
- Tagliavini F, Lievens PM-J, Tranchant C, Warter J-M, Mohr M, Giaccone G, Perini F, Rossi G, Salmona M, Piccardo P, Ghetti B, Beavis RC, Bugiani O, Frangione B, Prelli F (2001) A 7-kDa Prion Protein (PrP) fragment, an integral component of the PrP region required for infectivity, is the major amyloid protein in Gerstmann-Sträussler-Scheinker disease A117V. J Biol Chem 276(8):6009–6015. https://doi.org/10.1074/jbc.M007062200
- Theint T, Nadaud PS, Aucoin D, Helmus JJ, Pondaven SP, Surewicz K, Surewicz WK, Jaroniec CP (2017) Species-dependent structural polymorphism of Y145Stop prion protein amyloid revealed by solid-state NMR spectroscopy. Nat Commun 8(1):753. https:// doi.org/10.1038/s41467-017-00794-z
- Theint T, Nadaud PS, Surewicz K, Surewicz WK, Jaroniec CP (2017) 13C and 15N chemical shift assignments of mammalian Y145Stop prion protein amyloid fibrils. Biomol NMR Assign 11(1):75–80. https://doi.org/10.1007/s12104-016-9723-6
- Theint T, Xia Y, Nadaud PS, Mukhopadhyay D, Schwieters CD, Surewicz K, Surewicz WK, Jaroniec CP (2018) Structural studies of amyloid fibrils by paramagnetic solid-state nuclear magnetic resonance spectroscopy. J Am Chem Soc 140(41):13161–13166. https://doi.org/10.1021/jacs.8b06758
- Vanik DL, Surewicz KA, Surewicz WK (2004) Molecular basis of barriers for interspecies transmissibility of mammalian prions. Mol Cell 14(1):139–145. https://doi.org/10.1016/s1097 -2765(04)00155-8
- Young K, Clark HB, Piccardo P, Dlouhy SR, Ghetti B (1997) Gerstmann–Sträussler–Scheinker disease with the PRNP P102L mutation and valine at codon 129. Mol Brain Res 44(1):147–150. https://doi.org/10.1016/S0169-328X(96)00251-3

Publisher's Note Springer Nature remains neutral with regard to jurisdictional claims in published maps and institutional affiliations.

